ASME Journal of Engineering for Gas Turbines and Power
Online journal at:
https://asmedigitalcollection.asme.org/gasturbinespower

# Techno-Economic Analysis and Optimal Supercritical Carbon Dioxide Power Cycle Configuration for Novel Concentrating Solar Power Plants Adopting Tubular Fluidized Particles Central Receivers

**Dario Alfani**[1]
Department of Energy,
Politecnico di Milano,
Milano 20156, Italy
e-mail: dario.alfani@polimi.it

**Filip Sobic**
Department of Energy,
Politecnico di Milano,
Milano 20156, Italy
e-mail: filip.sobic@polimi.it

**Marco Astolfi**
Department of Energy,
Politecnico di Milano,
Milano 20156, Italy
e-mail: marco.astolfi@polimi.it

**Marco Binotti**
Department of Energy,
Politecnico di Milano,
Milano 20156, Italy
e-mail: marco.binotti@polimi.it

**Paolo Silva**
Department of Energy,
Politecnico di Milano,
Milano 20156, Italy
e-mail: paolo.silva@polimi.it

*Concentrating solar power (CSP) plants, thanks to the use of cost-competitive thermal energy storage, can provide back-up power guaranteeing a zero-emission alternative to conventional power plants and offer balancing services to the electrical grid. However, 2023 average CSP levelized cost of electricity (0.117 $/kWh) is still remarkably higher than other renewable technologies. Next-generation solar towers are expected to employ novel receiver technologies to reach temperatures above 700 °C, leading to improved efficiency of the power block and competitive techno-economic performance. In this context, the Horizon Europe POWDER2POWER project aims to demonstrate at MW-scale the operation of innovative tubular receivers adopting fluidized particles reaching temperatures of 750 °C, while ensuring intraweek storage at reduced cost, increasing CSP competitiveness and its value for the grid. For these applications, the adoption of supercritical carbon dioxide ($sCO_2$) power cycles is highly recommended thanks to their high efficiency, compactness of turbomachinery, and simple plant arrangement. This work aims to confirm the potential advantages of $sCO_2$ power blocks for CSP plants based on fluidized particles. A numerical model is developed to calculate the system overall efficiency and the capital cost for different cycle configurations, to identify the optimal techno-economic solution which minimizes the plant specific cost. The model implements ad hoc routines for component sizing and uses referenced cost correlations for power block and solar field components. Results enable to select the optimal $sCO_2$ cycle configuration and design parameters considering the tradeoff between solar-to-electricity efficiency and total investment cost of the plant.*
[DOI: 10.1115/1.4068464]

## 1 Introduction

Concentrating solar power (CSP) plants, thanks to the use of cost-competitive thermal energy storage (TES), represent a zero-emission alternative to conventional power plants to provide both dispatchable and baseload generation. These systems could thus help to overcome the main limits of variable renewable energy sources, such as photovoltaic systems and wind turbines, related to their intrinsic unpredictability [1]. Furthermore, the application of TES to CSP plants can lead to a reduction in the levelized cost of electricity (LCOE), thanks to a decrease in the power block (PB) size, for a given solar field surface, and an increase in the equivalent hours [2].

Current state-of-the-art CSP plants adopt a central receiver and use solar salts (60% $NaNO_3$–40% $KNO_3$) both as heat transfer fluid (HTF) and storage medium in a direct two-tanks storage system. The PB consists of a conventional steam Rankine cycle and typical maximum temperatures are limited to around 565 °C to avoid solar salts decomposition [3]. Unfortunately, as the average LCOE of CSP for 2023 is equal to 0.117 $/kWh [4], this technology still faces some challenges in competing economically with other forms of electricity generation systems on the market. For this reason, academic and industrial research on CSP is pushing toward central receiver technologies able to reach higher temperatures, of at least 700 °C, to achieve improved power block efficiencies (>50%) and to lower the LCOE below 0.06 $/kWh [5].

Turbo Expo, June 24–28, 2024. GT2024.
[1]Corresponding author.
Manuscript received October 22, 2024; final manuscript received November 11, 2024; published online May 22, 2025. Editor: Jerzy T. Sawicki.

While nitrate salts have been effectively demonstrated as HTF for maximum operating temperature around 565 °C (e.g., Crescent Dunes Solar Energy Project, Gemasolar), they are not suitable for higher operating temperatures due to decomposition [3], motivating the research of alternative carriers capable of withstanding and efficiently transferring heat at temperatures above 700 °C. Carbonate, chloride, or fluoride salts represent a potential alternative, yet their utilization introduces several challenges primarily related to severe corrosion issues, ultimately leading to increased equipment and maintenance expenditures [6].

Consequently, the concept of employing solid particle suspensions as HTF received attention thanks to their high specific heat capacity and their easy integration with hot and cold bulk storage systems. This solution does not feature rigid temperature constraints, even if still limited by the maximum admissible wall temperature of the receiver tubes, and it is characterized by lower parasitic power losses, thanks to the mechanical or pneumatic conveying of solid particles [7]. Additionally, the adoption of particles as heat transfer medium eliminates the need for electric tracing of pipes, decreasing both the capital and operating costs of the CSP plant. This concept has been thoroughly investigated by the H2020 NEXT-CSP project [8], the main outcomes of which are the starting point of the Horizon Europe POWDER2POWER (P2P) project, which started in October 2023 and is dedicated to developing and demonstrating the fluidized particle-driven CSP concept at MW-scale for both power and industrial heat production. In the P2P project, the adoption of supercritical carbon dioxide ($sCO_2$) Brayton cycles for the CSP plant power block would also be investigated. These power conversion systems are extensively researched from both academia and industry, mostly due to their high efficiency, compactness of turbomachinery, simple plant arrangement, no water consumption, high performance at part-load, and fast transients in operation [9–11]. This work considers different $sCO_2$ cycles coupled to a solar tower CSP plant with a fluidized particle-driven receiver and a TES system. A numerical model is developed to assess the main design parameters, the solar-to-electricity efficiency, and the capital cost for different cycle configurations, with the aim of identifying the optimal techno-economic solutions.

## 2 Methodology and Scope of Work

The objective of this work is to carry out a preliminary techno-economic assessment of a 20 $MW_{el}$ nominal capacity plant based on the P2P concept. A qualitative plant layout scheme is proposed in Fig. 1, from which it is possible to recognize the different components that compose the P2P plant.

The fluidized particles CSP plant is designed considering the location of Seville (37.4 deg N, 5.9 deg W), in Spain, being one of the most promising sites in Europe as demonstrated from the numerous CSP projects here developed (e.g., the Gemasolar, the PS10, and the PS20 plants).

Due to the significant interactions among the different plant components, it is not possible to design them individually without considering the effects on the overall plant efficiency and investment cost. For this reason, the methodology briefly outlined in Fig. 2 has been followed.

First, the heliostat field is generated in SolarPILOT [12] and then exported to SolTrace [13], to produce the heat flux map on the receiver panels which is then provided as an input for the receiver thermal model. The thermal efficiency of the receiver is then obtained through numerical simulations carried out with a MATLAB thermal model for a wide range of fluidized particle inlet and outlet temperatures. On the other hand, the power block has been designed by means of a MATLAB + REFPROP V10 model, considering four different cycle configurations (see Sec. 2.2), air-cooling with a design ambient temperature of 35 °C, and a fixed cycle power output of 20 $MW_{el}$.

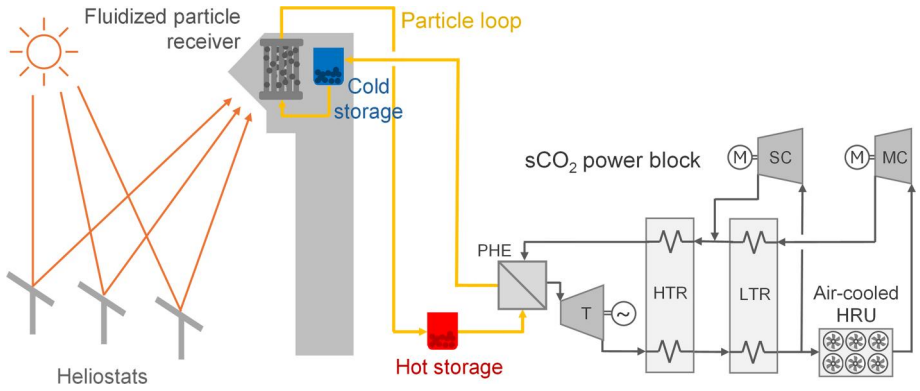


**Fig. 1 POWDER2POWER plant scheme adopting a recompressed $sCO_2$ power block**

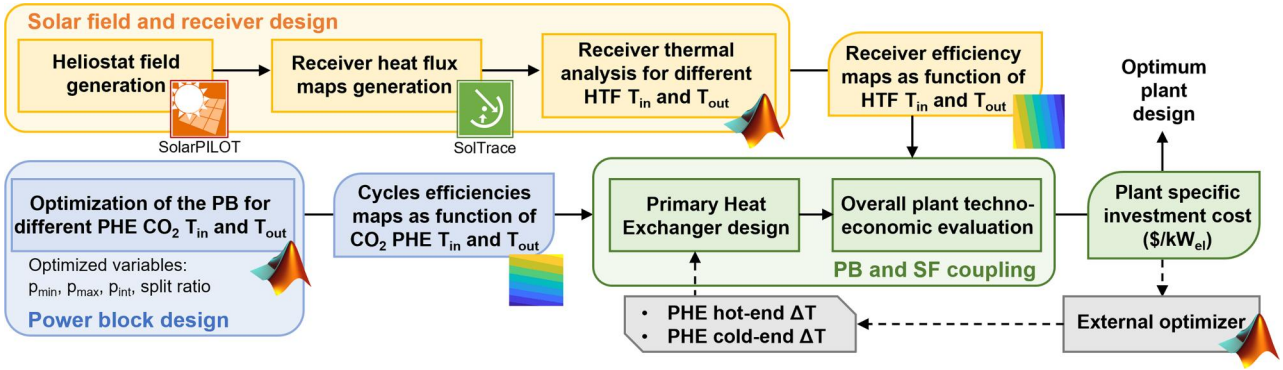


**Fig. 2 Flowchart of the methodology employed to design the overall P2P plant**

**Table 1 Assumptions for the solar field**

| Parameter | Value |
|---|---|
| **Solar Field** | |
| Location | Seville, Spain |
| Design point | Solar noon, June 21st |
| Design direct normal irradiance, W/m$^2$ | 970 |
| Tower height, m | 193 |
| Heliostat size, m × m | 7 × 7 |
| Heliostat reflectivity | 0.92 |
| Heliostat reflected image error, mrad | 1.8 |
| Aiming strategy | Image size priority $\sigma = 1.5$ |
| **Receiver** | |
| Impinging power on the aperture, MW | 140 |
| Horizontal acceptance angle, deg | 120 |
| Cavity aperture size, m × m | 6.3 × 7.8 |
| Cavity tilt, deg | 30 |
| Number of receiver panels | 5 |
| Receiver panel size, m × m | 6.1 × 5.5 |
| **HTF and TES** | |
| Hours of storage, h | 13 |
| HTF and storage medium | Olivine |

For each cycle configuration, several design cases are obtained by parametrically varying the inlet and outlet $CO_2$ temperature at the primary heat exchanger (PHE), while the cycle pressure levels and the split ratio are optimized at all times, as explained in detail in Sec. 2.2.

Along with the thermodynamic streams conditions, the power balances, and the cycle performances, also a preliminary estimate of the size and cost of the heat exchangers is computed, except for the primary heat exchanger as it requires the definition of the HTF temperature profile. The power block performance maps obtained for the different cycle configurations are then coupled to the solar field and receiver by optimizing the cold- and hot-end temperature difference of the primary heat exchanger, thus determining the inlet and outlet temperature of the HTF.

The objective function of this optimization is the specific investment cost of the plant ($/kW$_{el}$), a figure of merit which allows to consider the tradeoff between the plant performance (influenced by the power block, the particle conveying system, the receiver, etc.) and the investment cost of the plant. The modeling of each plant subsection is described in detail in the next paragraphs.

**2.1 Solar Field and Receiver.** The solar field and receiver design is performed through the combined use of SolarPILOT and SolTrace. A semicylindrical cavity, for updraft fluidized particle receivers, is selected in this work according to Ref. [14]. The receiver is scaled up considering a solar multiple (SM) of 2.8 and first guess efficiencies for the power block and the receiver of 50% and 80%, respectively. In SolarPILOT, the solar field is designed considering a simplified rectangular target, tilted downwards by 30 deg, with a size equal to the aperture of the cavity of the receiver (see Table 1).

All the thermal losses related to particles conveying and storage system are neglected, and they will be considered in future investigations of the technology. Consequently, the estimated power to the aperture is equal to 140 MW, concentrated on an aperture area of 48.8 m$^2$ (7.8 m of height and 6.3 m of width).

The tower height is equal to 193 m, as for the Gemasolar plant, while the heliostat field adopts square mirrors (7 m × 7 m) with optical quality of 1.8 mrad as reported in Ref. [15]. All the main assumptions related to the design of the solar field, the receiver, and the thermal energy storage are reported in Table 1.

*Description of the Solar Field Model.* The solar field generated in SolarPILOT is then exported to SolTrace, where the detailed panels geometry (see Table 1) is inserted adding a subsequent optical stage. For simplicity, the internal walls of the cavity are not simulated, and all the radiation entering the cavity but missing the panels is assumed to be evenly reflected by the passive walls onto the receiver panels with a reflectivity of 0.78 [14].

Receiver geometry is retrieved from Ref. [14] and then scaled up proportionally to the required power, with the only difference being that the receiver panels inside the cavity are translated vertically to maximize the collected incident radiation. Since to keep the proportions the required height of the panels would be 11 m, which exceeds the tube height limit of 7 m given in Ref. [14], it is decided to split the absorbing surface in two 5.5 m high receivers one on top of the other (see Fig. 3).

The heat flux map on the panels is then provided as an input for the receiver thermal model.

*Description of the Receiver Thermal Model.* The receiver thermal model for tubular billboard receivers from Ref. [16], and based on tools presented in Ref. [17], is adopted and modified to consider the presence of the cavity.

Due to the high resulting wall temperatures in the receiver, Inconel 601 is selected as the material for the tubes. Accordingly, the maximum peak heat flux is limited to around 500 W/m$^2$ [7]. The two-dimensional steady-state thermal model takes into account the effect of both radiative and convective losses. For simplicity, the effect of the cavity is considered only by multiplying the view factor between the tube and the ambient by the view factor between the whole receiver area and the aperture. Therefore, the radiative exchange with the reflective surfaces inside the cavity and other tubes, except the neighboring tube, is neglected. Convective losses are assumed to take place only from the surface of the tubes, and the convective heat transfer coefficient is assumed equal to 10 W/m$^2$K, as recommended in Ref. [14]. The heat transfer coefficient between the fluidized particles and the receiver tubes has been assumed constant and equal to 1200 W/m$^2$K [18], and the thermal conductivity of Inconel 601 has been assumed equal to 26.1 W/mK.

From the NEXT-CSP project experience, olivine has been selected as HTF and storage material for its thermal properties, its inert and widely available nature, and its reasonable cost [7].

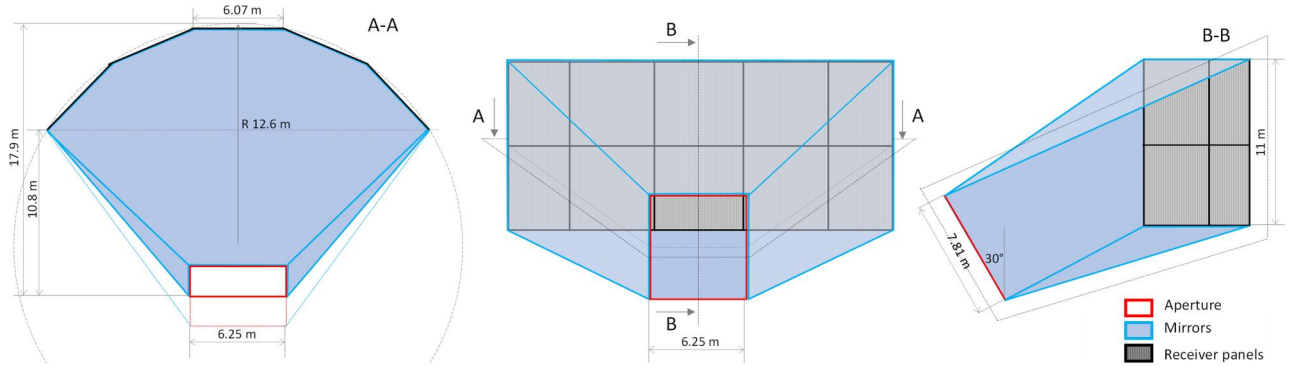


**Fig. 3 Fluidized particles cavity receiver geometry**

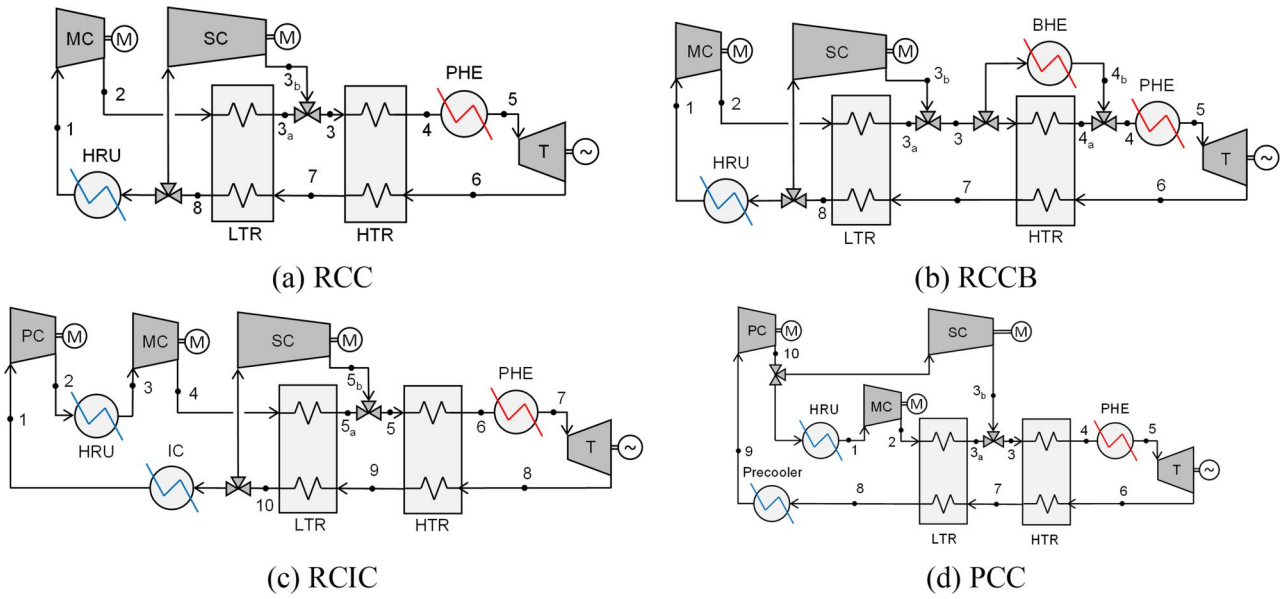


**Fig. 4 Schematic of the CSP $sCO_2$-based plant configurations: (*a*) RCC, (*b*) RCCB, (*c*) RCIC, and (*d*) PCC**

**2.2 Power Block Configurations and Modeling.** The power block has been designed considering a power output equal to 20 $MW_{el}$ including the air-cooling auxiliaries electrical consumption, while not considering the power required for the particles handling and conveying. As depicted in Fig. 2, this consumption will be included in the next step of the plant design as a result of the coupling of the power block to the solar field and receiver, which defines the particles mass flow rate and thus electric requirements for their handling and conveying. A MATLAB + REFPROP V10 numerical model has been employed to calculate the efficiency and to preliminarily size the heat exchangers for four different $sCO_2$ Brayton cycle configurations: the recompressed cycle (RCC), the recompressed cycle with main compressor intercooling (RCIC), the recompressed cycle with high temperature recuperator (HTR) bypass (RCCB), and the partial cooling cycle (PCC). It has been decided to not include the simple recuperated cycle as its conversion efficiency for high temperature applications was too low to achieve to competitive solutions. A schematic of each cycle layout is depicted in Fig. 4. Recompressed cycle is generally considered the optimal configuration for high temperature applications thanks to its high conversion efficiency, obtained through an efficient internal recuperation process [19]. However, this characteristic leads to a high $CO_2$ temperature at the inlet of the PHE, which limits its potential for CSP applications, as a higher return temperature of the HTF leads to higher thermal losses of the receiver and a larger size of the TES for the same nominal capacity. A possible solution to this issue is represented by a partial bypass of the HTR, where a fraction of the $CO_2$ is split just before entering the HTR cold side (point 3 in Fig. 4(*b*)) and it is then heated up in the bypass heat exchanger (BHE) by further cooling the HTF (point 4b). The bypass stream is then mixed with the $CO_2$ main flow at the HTR cold side outlet (point 4a) before entering the PHE (point 4). This solution allows to reduce the average temperature of heat introduction in the power cycles at the expense of an additional heat exchanger and a higher heat transfer surface in the HTR, as the heat capacities of the hot and cold streams become more similar [11,20].

Moreover, another difficulty related to the adoption of $CO_2$ supercritical cycles for CSP applications is related to the high ambient temperatures and water scarcity that characterize locations with a high direct normal irradiance. This aspect implies the adoption of air-cooled heat rejection units (HRUs) and relatively high compressor inlet temperatures of the cycle, leading to lower $CO_2$ densities along the compression process and therefore to a higher compressor power consumption. Considering that the average ambient temperatures during summer in Seville are around 35 °C, a minimum cycle temperature of 45 °C has been considered.

The RCIC and PCC configurations alleviate the problem thanks to a lower average compression temperature obtained by splitting the compression into two phases, among which an intercooling of the $CO_2$ is placed. This feature also allows these configurations to have a lower temperature at compressor outlet, and thus, for the same level of internal heat recuperation, a lower temperature at PHE inlet, leading to the aforementioned advantages. All the mixing processes of the different configurations (see Fig. 4) have been set as isothermal by varying the $CO_2$ mass flow rates sent to the secondary compressor or to the bypass heat exchanger, as this solution allows to minimize the mixing irreversibility and thus to optimize the cycle efficiency [21].

The assumed pressure drops (computed as percentage of the inlet pressure) are reported in Table 2. For the RCCB configuration, the pressure drop in the BHE is considered equal to that of the HTR cold side, so that an isothermobaric mixing of the two $CO_2$ streams is assumed.

Constant values of isentropic efficiencies of the turbomachinery equal to 90% and 85% are set for the turbine and the compressors [22], respectively. An electrical motor efficiency equal to 97% is considered for each compressor, while the electrical generator efficiency of the turbine is set to 98.5%, as recommended in Ref. [22]. Pinch point temperature difference ($\Delta T_{pp}$) of the low

**Table 2 Assumption for the $sCO_2$ power block**

| Parameter | Value |
|---|---|
| Net cycle power output, $MW_{el}$ | 20 |
| Minimum cycle temperature, °C | 45 |
| Maximum cycle allowable pressure, bar | 250 |
| Isentropic turbine efficiency | 90% |
| Isentropic compressors efficiency | 85% |
| LTR pinch point $\Delta T$, °C | 5 |
| HTR pinch point $\Delta T$, °C | 5–75 |
| PHE pressure drops | 1% |
| HRU/IC pressure drops | 1% |
| LTR/HTR hot side pressure drops | 0.5% |
| LTR/HTR cold side pressure drops | 0.1% |
| Motor/generator efficiencies | 97%/98.5% |
| $\dot{W}_{el,HRU}/\dot{Q}_{HRU}$, $MW_{el}/MW_{th}$ | 0.85% |

temperature recuperator (LTR) has been fixed to the assumed technological limit, equal to 5 °C, coherently with the results obtained in Ref. [23].

To finalize the power cycle design, it is necessary to define some additional parameters, namely:

- The cycle minimum pressure and the pressure ratio of the main compressor for the RCIC and PCC configurations. Those parameters have been optimized for each single design to maximize the cycle thermodynamic efficiency using an internal optimization routine based on the *patternsearch* algorithm [24].
- Due to the lack of investment cost correlations which consider the actual metal mass of the heat exchangers, which is function of the tube thicknesses, the maximum operating pressure of the cycle has been set to a technologically feasible value of 250 bar [23].
- The maximum temperature of the cycle and the HTR $\Delta T_{pp}$ have been varied in a specific range by means of a parametric analysis with the aim of investigating different power block designs in terms of costs and cycle efficiency. Cycle maximum temperature has been varied between 600 °C and 740 °C, while the HTR $\Delta T_{pp}$ has been varied between 5 °C and 75 °C. The higher the internal cycle recuperation (lower HTR $\Delta T_{pp}$), the higher the cycle efficiency but also the narrower the temperature range of heat introduction in the cycle.

It is thus possible to notice that, for a fixed HTF PHE inlet temperature, this aspect results in a lower temperature difference also for the HTF. As already mentioned, in a CSP plant, this aspect leads to a narrower temperature difference of the storage system and so to a larger inventory of storage medium and to a higher investment cost of the TES system. To address this aspect, a TES cost correlation is employed in this work as a function of the storage volumetric size and temperature, as explained in Sec. 2.3. Furthermore, the convective and radiative thermal losses of the receiver increase because the HTF average temperature is higher for a given maximum temperature. This aspect is considered in this work thanks to the receiver thermal model presented in Sec. 2.1.

The final output and objective function of the power block model is the net cycle efficiency computed as the ratio of the net power output of the $sCO_2$-based power block and the thermal input to the cycle, as reported in Eq. (1). The HRU auxiliaries work related to the cooling air fan consumption ($\dot{W}_{el,HRU}$) is computed as 0.85% of the thermal duty that must be rejected by the heat exchanger to the environment [24]

$$\eta_{cycle} = \frac{\dot{W}_{net,cycle}}{\dot{Q}_{in,cycle}} = \frac{\dot{W}_{turb,el} - \sum \dot{W}_{comp,el} - \dot{W}_{el,HRU}}{\dot{Q}_{in,cycle}} \tag{1}$$

Parasitic consumption related to air compression for fluidization is neglected, as well as the thermal losses linked to the flow rate of fluidization air. Related to this last aspect, it must be noticed that these losses can be significantly mitigated by recirculating a portion of the fluidization air, as suggested in Ref. [7].

**2.3 Techno-Economic Analysis.** The cost correlations for each component of the power block are taken from Weiland et al. [25], apart for the PHE cost correlation which is taken from Ref. [26], considering the cost of a conventional Shell&Tube heat exchanger and applying a cost multiplier equal to 5 with respect to stainless steel [27] related to the adoption of nickel-based superalloys due to the high operating temperatures. For the solar field (heliostats, land occupation, and tower), the cost correlations adopted in System Advisor Model (SAM) [28] and already reported in Ref. [23] are used. It must be noted that the fluidized particle solar receiver is more difficult to design and operate than a molten salt receiver in certain aspects, such as the greater complexity moving particles through fluidization with respect to pumping a liquid. Conversely, it is less complex in other regards, notably the absence of corrosion or freezing concerns, even if erosion issues must be dealt with. Thus, due to the uncertainty related to the estimation of its cost, the same cost per receiver surface adopted in SAM for the molten salt technology has been adopted [28].

For the thermal energy storage, temperature-dependent area-specific cost correlation proposed in Ref. [29] has been employed. The total amount of olivine necessary to achieve 13 h of storage capacity is computed assuming a density of olivine equal to 3300 kg/m$^3$ and a specific heat capacity as a function of temperature as reported in Ref. [30]. An extra 10% particle mass is added to account for the amount in other components of the plants, as suggested in Ref. [31]. Then, considering a void faction of 0.52 [30] the total volumes of the hot and cold storage hoppers are computed. Finally, cylindrical hoppers are assumed with a height-to-internal diameter ratio of 2 [31], and the total insulated surface is computed for both the hot and the cold storage. A specific cost of olivine equal to 0.1 $/kg is then employed to account for the cost of HTF inventory. For the particle conveying, due to the lack of accurate literature correlations, the same cost correlation reported in Ref. [32] for the falling particle receiver technology has been considered.

Finally, contingencies and engineering, procurement, and construction costs are considered equal to 7% and 11%, respectively, of the direct capital costs [28], while a factor equal to 20% is considered for the balance of plant.

## 3 Results and Discussion

**3.1 Solar Field and Receiver.** The solar field layout and heat flux map obtained through the combined use of SolarPILOT and SolTrace are reported in Figs. 5 and 6. The solar field consists of 4259 heliostats and has an average optical efficiency of 65.0%, largest loss being the "spillage" (reflected solar radiation not hitting the aperture due to manufacturing and tracking errors), as the size of the aperture is relatively small compared to the size of the receiver.

The thermal efficiency of the receiver $\eta_{rec}$ obtained through the thermal model simulations is reported in Fig. 7. These results have been then used to obtain a polynomial interpolating function to define the receiver thermal efficiency, as reported in Eq. (2), where $T_{HTF,in}$ and $T_{HTF,out}$ are the HTF inlet and outlet temperatures, respectively,

$$\eta_{rec} = 0.9235 - 1.59 \times 10^{-5} \cdot T_{HTF,in} - 4.45 \times 10^{-5} \cdot T_{HTF,out} - 2.01 \times 10^{-8} \cdot T_{HTF,in}^2 - 1.14 \times 10^{-8} \cdot T_{HTF,in} \cdot T_{HTF,out} \tag{2}$$

**3.2 Power Block.** All the results of the thermodynamic optimization are reported in Fig. 8, highlighting the comparable

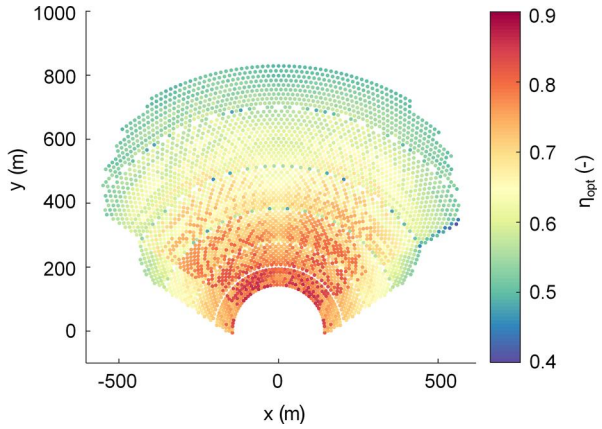


**Fig. 5 Solar field layout and optical efficiency at design conditions**

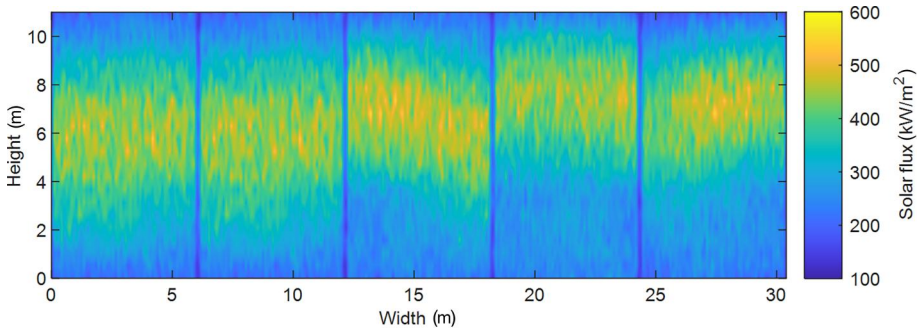


**Fig. 6 Receiver heat flux map at design conditions**

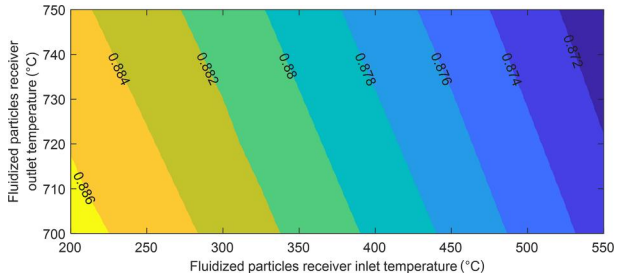


**Fig. 7 Receiver efficiency as function of the HTF inlet and outlet temperatures**

cycle thermodynamic efficiencies obtained by the four configurations and thus the very similar thermal power input. The regions of admissible points do not cover the full range because the two parameters (maximum cycle temperature and HTR $\Delta T_{pp}$) are linked together: once the maximum cycle temperature is fixed and the HTR $\Delta T_{pp}$ is selected in its variability range, the cycle minimum pressure is optimized resulting in a specific turbine outlet temperature and PHE inlet temperature (considering the range of HTR $\Delta T_{pp}$). Main differences are related to the RCCB configuration that, with respect to the other three configurations: (i) allows entering in the heat introduction heat exchanger (BHE) at much lower temperatures (low as 179 °C) thanks to the recuperator bypass, (ii) is optimized in performance for the minimum primary heat exchanger inlet temperature rather than for the maximum one, and in conclusion (iii) reaches maximum efficiency for a much larger temperature span in the heat introduction process (555 °C versus around 200 °C) thus potentially leading to lower cost of TES. It is worth highlighting that in case of RCCB the minimum temperature difference in the heat introduction process is at the BHE outlet–PHE inlet according to the different $CO_2$ mass flow rates at cold side of the two heat exchangers. Thus, even if the bypass heat exchanger allows to improve the HTF cooling with respect to the RCC configuration, it is not possible to achieve HTF minimum temperatures close to the $CO_2$ BHE inlet temperature due to the pinch point constraint at the BHE outlet–PHE inlet section. The best results are obtained by the RCIC configuration, with a net cycle efficiency of 50.25% for a maximum cycle temperature of 740 °C and a HTR $\Delta T_{pp}$ of 5 °C (corresponding to a $CO_2$ PHE inlet temperature of 556.8 °C), which slightly overtakes the performance of the RCC and RCCB configurations (49.52%). These results are then combined with the receiver efficiency map reported in Fig. 7 to obtain the overall solar-to-electricity efficiency $\eta_{sun2el}$, defined as reported in Eq. (3), where $\eta_{opt}$ is the solar field optical efficiency and $\eta_{aux,SF}$ is the efficiency related to the auxiliaries consumption, namely, the particle conveying, which is computed adopting a 80% efficiency with respect to the mechanical power required for particle lifting [33]

$$\eta_{sun2el} = \eta_{opt} \cdot \eta_{rec} \cdot \eta_{cycle} \cdot \eta_{aux,SF} \tag{3}$$

**3.3 Techno-Economic Analysis.** The information available from solar field and receiver analysis are eventually combined with those related to power plant design and performance to assess a preliminary techno-economic analysis. The parameter selected as figure of merit for this analysis is the plant specific cost in \$/kW$_{el}$, calculated as the sum of all the system costs (i.e., solar field, receiver, TES and solid particles handling devices, power block, and balance of plant) divided by the net plant electrical power equal to the difference between the net power delivered by the $sCO_2$-based power block (always set to 20 MW$_{el}$) and the power required by the particle handling systems (divided by the SM in order to account for the correct amount of solid displaced when the power plant operates

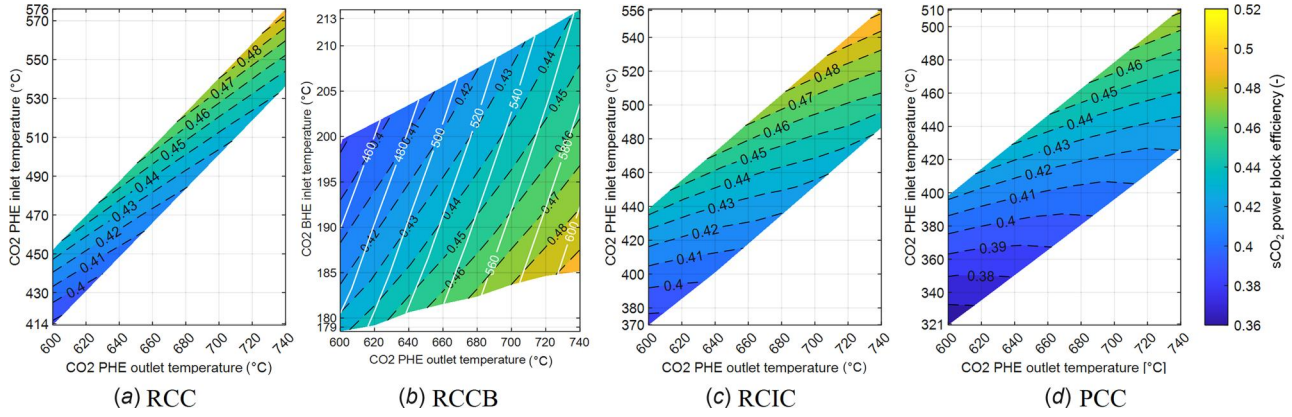


**Fig. 8 Cycle efficiency of the different $sCO_2$-based power blocks as function of the PHE (BHE for the RCCB) inlet and PHE outlet temperature. The solid lines for the RCCB configuration indicate the $CO_2$ PHE inlet temperature. (*a*) RCC, (*b*) RCCB, (*c*) RCIC, and (*d*) PCC.**

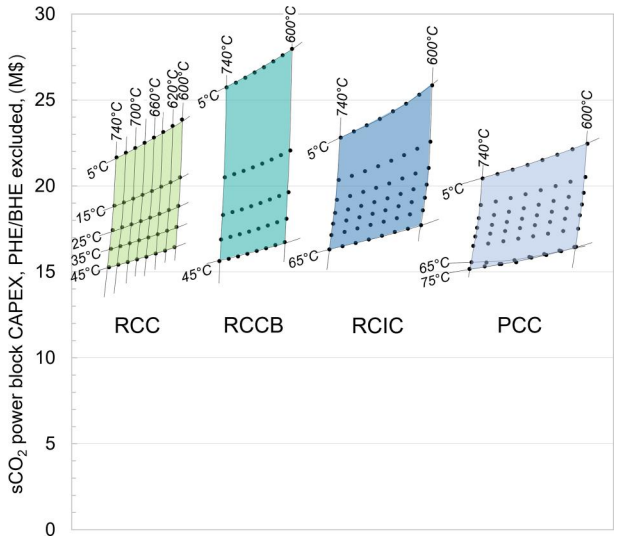


**Fig. 9 $sCO_2$-based PB investment cost (not including the PHE+BHE)**

at nominal condition). The plant specific cost has been preferred to the LCOE since the quantification of this latter index would require the knowledge of the annual energy yield. Considering that the SM and TES design number of hours is the same for all the investigated cases and that all the cycles adopt the same heat rejection unit type, the number of equivalent operating hours is expected to be similar for all the plants. For this reason, the analysis based on the specific plant cost should lead to similar conclusions with respect to a more detailed analysis in which the LCOE is used as figure of merit. The plant specific cost for each different design case is calculated with the procedure already presented in Sec. 2. First, the cost of each $sCO_2$ PB component but the PHE (or BHE+PHE for RCCB configuration) is calculated adopting the correlations reported in Sec. 2.3. Results are depicted in Fig. 9, and it is possible to highlight that, not including the PHE+BHE, all the $sCO_2$ cycle configurations show a comparable investment cost. An exception is represented by the RCCB cases characterized by a HTR $\Delta T_{pp}$ of 5 °C, which have a capital cost appreciably higher than the other systems, due to exponential growth of the recuperators cost, in particular of the HTR, which design for this configuration is pinched on both the cold and hot side.

*Primary Heat Exchanger Design and Definition of Heat Transfer Fluid Temperature Profile*. Then, the PHE (or BHE+PHE for RCCB configuration) design is obtained through an optimization procedure that varies the heat exchanger cold- and hot-end temperature differences, thus defining the minimum and maximum temperature of the fluidized particles, in order to minimize the specific cost of the plant. For sake of simplicity, the PHE global heat transfer coefficient is considered constant and equal to 800 W/m$^2$K [7]. The optimization always sets the maximum temperature of the HTF to the maximum value compatible with the receiver materials (750 °C), since reducing this parameter allows from one side to increase the receiver thermal efficiency (improvement is however very limited according to Fig. 7) but on the other one it translates into various penalizing effects such as higher TES cost, an increase of the fluidized particles mass flow rate, and a larger PHE surface. Differently, for a given thermodynamic cycle, the lower the minimum temperature of fluidized particles, the higher the heat exchanger surface and cost, while on the contrary the HTF mass flow rate reduces (leading to a particle conveying equipment cost and consumption reduction), the TES dimension and cost decreases, and the receiver thermal efficiency slightly increases. This last effect also impacts the size of the heliostat field which is scaled on the receiver incident power by keeping the same optical efficiency (i.e., minor variation in reflecting area and last mirror distance from receiver do not impact the solar field efficiency appreciably). The different trends of components costs and the impact of auxiliaries consumption on the net plant power output lead to a tradeoff analysis on plant specific cost.

Maps of specific cost are reported in Fig. 10: for each plant configuration, it is possible to note that the minimum specific cost is generally obtained for the plant that finds the best tradeoff between the need of minimizing the cost of the solar field and TES section without penalizing excessively the performance of the plant.

Figure 11 depicts the fluidized particles mass flow rate (dotted line on contour plot) and PHE outlet temperature (solid lines) for the different P2P plant designs as function of the $CO_2$ PHE (BHE for the RCCB) inlet and PHE outlet temperature for the four different power block configurations. As already reported in previous studies [34], the PCC allows to obtain lower HTF temperatures at receiver inlet thanks to the greater pressure ratio of the turbine, which leads to lower temperature at turbine outlet and a limited internal recuperation with respect to configurations based on the recompressed cycle. As mentioned in Sec. 2.2, this aspect leads to higher receiver efficiency and lower costs of the storage. However, it must be noted that, as the thermal efficiency of this kind of receiver is less sensitive to HTF temperature variation than other technologies thanks to the presence of the cavity (which reduces both the radiative and convective losses), and the fact that the storage cost accounts for just for a small fraction of the plant investment cost, these two advantages are not actually leading to a significant improvement in the techno-economic performances of the plant, and all the cycle configurations are able to reach minimum values of the specific plant investment cost in the same range, namely, between 8450 and 8600 $/kW.

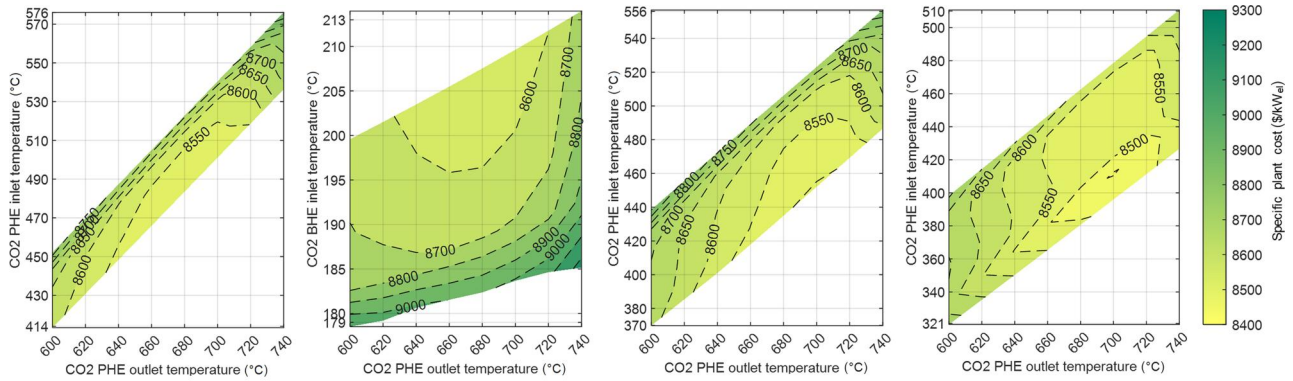


**Fig. 10 Specific plant cost in $/kW$_{el}$ of the different P2P plant designs as function of power block configuration, $CO_2$ PHE (BHE for the RCCB) inlet and PHE outlet temperature: (*a*) RCC, (*b*) RCCB, (*c*) RCIC, and (*d*) PCC**

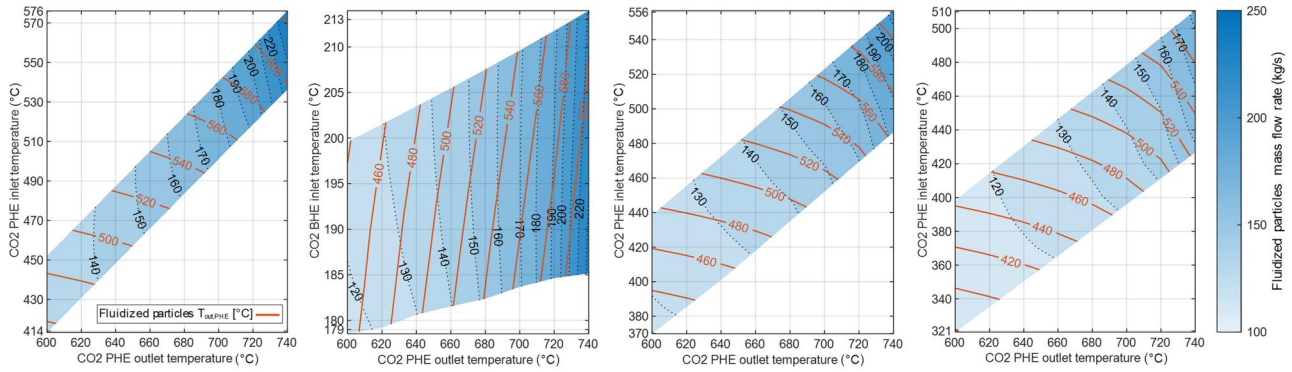


(*a*) RCC (*b*) RCCB (*c*) RCIC (*d*) PCC

**Fig. 11 Optimal fluidized particles mass flow rate (dotted line, contour) and PHE outlet temperature (solid lines) of the different P2P plant designs as function of power block configuration, $CO_2$ PHE (BHE for the RCCB) inlet and PHE outlet temperature: (*a*) RCC, (*b*) RCCB, (*c*) RCIC, and (*d*) PCC**

Main results for the minimum specific cost design cases for each of the four plant configurations are reported in Table 3. It is interesting to notice that the PCC, which is the cycle configuration achieving the lowest specific cost (8446.8 $/kW), is also the one featuring the lowest power block (41.26%) and sun-to-electricity efficiencies (23.05%), underlining another time the fact that there is no actual need to push to really high values the efficiency of the power block at the expense of increased investment costs. Table 4 depicts the capital cost breakdown for the minimum specific cost design for each of the four plant configurations. It is possible to appreciate that the cost related to receiver, the tower, and the heliostat field is much larger than $sCO_2$ power block related costs (PHE included).

Despite the lower efficiency, the PCC configuration is able to reach the minimum specific cost thanks to the lower TES and PB costs. The first is due to the lower HTF minimum temperature, as previously stated, while the second can be attributed to the lower $CO_2$ mass flow rate and internal recuperation of the PCC configuration, which leads to lower costs of the recuperators.

It must be finally noted that, due to the intrinsic uncertainties associated with component cost correlations, it results evident that despite it is possible to identify an optimal PB configuration able to minimize the plant specific cost, the overall results tend to converge, making the different configurations comparable from a techno-economic perspective. Thus, the final selection criteria of the PB should also take into account further considerations, such as aspects related to layout complexity and part-load flexibility and performance.

**Table 3 Results for the optimal case for each different cycle configuration**

| Parameter | RCC | RCCB | RCIC | PCC |
|---|---|---|---|---|
| $CO_2$ $T_{in,PHE}$, °C | 483.5 | 510.2 | 452.1 | 411.9 |
| $CO_2$ $T_{out,PHE}$, °C | 680 | 680 | 700 | 700 |
| $CO_2$ $T_{in,BHE}$, °C | — | 207.52 | — | — |
| $CO_2\dot{m}$, kg/s | 192.6 | 192.6 | 150.1 | 133.8 |
| $p_{min}$, bar | 93.88 | 93.88 | 66.75 | 56.03 |
| $p_{max}$, bar | 250 | 250 | 250 | 250 |
| $p_{int}$, bar | — | — | 68.10 | 97.14 |
| Particles $T_{in,PHE}$, °C | 750 | 750 | 750 | 750 |
| Particles $T_{out,PHE}$, °C | 528.1 | 550.35 | 507.5 | 481.9 |
| Particles $T_{out,BHE}$, °C | — | 519.3 | — | — |
| Particles $\dot{m}$, kg/s | 161.2 | 155.0 | 144.8 | 135.6 |
| $\dot{W}_{turb}$, MW | 28.22 | 28.22 | 29.10 | 29.51 |
| $\dot{W}_{main\ comp}$, MW | 6.72 | 6.72 | 5.15 | 4.51 |
| $\dot{W}_{sec\ comp}$, MW | 0.63 | 0.63 | 0.59 | 0.00 |
| $\dot{W}_{precomp}$, MW | — | — | 2.45 | 4.06 |
| $\dot{W}_{HRU}$, $kW_{el}$ | 227.7 | 227.7 | 220.1 | 234.0 |
| $\dot{Q}_{PHE}$, MW | 47.66 | 41.24 | 46.82 | 48.48 |
| $\dot{Q}_{BHE}$, MW | — | 6.42 | — | — |
| $\dot{Q}_{rec,thermal}$, MW | 133.46 | 133.46 | 131.11 | 135.73 |
| $\dot{Q}_{rec,incident}$, MW | 153.12 | 153.05 | 150.27 | 155.35 |
| $\dot{Q}_{sun}$, MW | 235.56 | 235.45 | 231.17 | 239.01 |
| $\eta_{cycle}$, % | 41.96 | 41.96 | 42.71 | 41.26 |
| $\eta_{opt}$, % | 65.0 | 65.0 | 65.0 | 65.0 |
| $\eta_{aux,SF}$, % | 98.09 | 98.17 | 98.29 | 98.40 |
| $\eta_{rec}$, % | 87.16 | 87.20 | 87.26 | 87.37 |
| $\eta_{sun2el}$, % | 23.32 | 23.35 | 23.81 | 23.05 |

**Table 4 Cost breakdown for the optimal case for each different cycle configuration**

| Cost, M$ | RCC | RCCB | RCIC | PCC |
|---|---|---|---|---|
| Turbine | 4.08 | 4.08 | 4.15 | 4.18 |
| Main compressor | 2.63 | 2.63 | 2.37 | 2.24 |
| Secondary compressor | 1.02 | 1.02 | 1.00 | 0.07 |
| Precompressor | — | — | 1.76 | 2.15 |
| PHE | 3.62 | 3.37 | 3.66 | 3.55 |
| HRU | 1.41 | 1.41 | 0.66 | 1.20 |
| Inter/precooling | — | — | 1.21 | 0.55 |
| LTR | 2.54 | 2.54 | 1.95 | 1.51 |
| HTR | 1.80 | 2.13 | 0.97 | 0.93 |
| HTR bypass | — | 0.78 | — | — |
| Generator | 0.68 | 0.68 | 0.69 | 0.69 |
| Motors | 1.57 | 1.57 | 2.06 | 1.94 |
| Heliostats | 30.84 | 30.83 | 30.27 | 31.29 |
| Land | 0.60 | 0.60 | 0.59 | 0.61 |
| Site improvements | 3.89 | 3.88 | 3.81 | 3.94 |
| Receiver | 34.95 | 34.95 | 34.95 | 34.95 |
| Tower | 25.97 | 25.97 | 25.97 | 25.97 |
| Hot storage | 2.11 | 2.06 | 1.97 | 1.88 |
| Cold storage | 1.90 | 1.85 | 1.77 | 1.69 |
| Particles inventory | 0.83 | 0.80 | 0.75 | 0.70 |
| Particles conveying | 0.40 | 0.40 | 0.40 | 0.41 |
| Balance of plant | 24.17 | 24.31 | 24.19 | 24.09 |
| Contingencies | 13.29 | 13.37 | 13.30 | 13.25 |
| Engineering, procurement, and construction | 8.46 | 8.51 | 8.47 | 8.43 |
| Total, M$ | 166.77 | 167.74 | 166.90 | 166.22 |
| Specific cost, $/kW | 8501.7 | 8544.6 | 8491.5 | 8446.8 |

## 4 Conclusions

In the present work, a preliminary techno-economic optimization of a solar power tower based on a fluidized particle receiver and a $sCO_2$ power block has been performed. The results of the design and optimization of the plant subsections have been reported in the form of parametric performance maps, highlighting the strong tradeoff

between plant investment cost and solar-to-electricity plant efficiency. The power block performances of four different cycle configurations are coupled to the solar field and receiver efficiencies by optimizing the design of the primary heat exchanger, namely, selecting the cold- and hot-end temperature difference of the component, and thus determining the inlet and outlet temperature of the HTF. The objective function of this optimization is the specific investment cost of the plant ($/kW$_{el}$), a figure of merit which allows to consider the tradeoff between the plant performances (influenced by the power block, the conveying system, the receiver, etc.) and the economic competitiveness of the plant.

Of the four studied cycle configurations, the PCC showed the most promising results from a techno-economic point of view, as it reached the lowest plant specific cost with a value of 8446.8 $/kW, even if it is characterized by a lower solar-to-electricity efficiency, equal to 23.05%. The cost breakdown of this cycle configuration highlighted how the lower average temperature of heat introduction allows to decrease the storage cost, as well as the lower $CO_2$ mass flow rate and internal recuperation of the PCC configuration lead to lower costs of the recuperators. Furthermore, the lower particle temperature at receiver inlet allows to achieve a slightly higher receiver thermal efficiency. Future improvements of this work will focus on a more detailed description of the radiative heat exchange model of the receiver cavity and on the use of a variable internal heat transfer coefficient for the fluidized particles in the receiver tubes: these modifications would allow a more accurate receiver thermal efficiency prediction. The analysis would also benefit from an improvement in the PHE model, which should be able to accurately compute the number of heat exchanger stages and to properly estimate the global heat transfer coefficient. Another future improvement will consist in the introduction of more accurate heat exchangers cost correlations considering their actual metal masses, to also optimize the cycle pressure levels. Moreover, the extension of the optimization routine with a detailed yearly simulation to compare the different options from an LCOE point of view is foreseen.

## Acknowledgment

The current work has been developed for the POWDER2POWER project,[2] which has received funding from the European Union's Horizon Europe research and innovation programme under Grant Agreement No. 101122347.

This study was carried out within the NEST—Network 4 Energy Sustainable Transition (D.D. 1243 02/08/2022, PE00000021) and received funding under the National Recovery and Resilience Plan (NRRP), Mission 4 Component 2 Investment 1.3, funded from the European Union—NextGenerationEU. This paper reflects only the authors' views and opinions, neither the European Union nor the European Commission can be considered responsible for them.

## Funding Data

- European Union's Horizon Europe research and innovation programme (Grant Agreement No. 101122347; Funder ID: 10.13039/100004431).
- National Recovery and Resilience Plan (NRRP), Mission 4 Component 2 Investment 1.3, funded from the European Union—NextGenerationEU (ID: PE0000021).

## Data Availability Statement

The datasets generated and supporting the findings of this article are obtainable from the corresponding author upon reasonable request.

[2]https://powder2power-project.eu/

## Nomenclature

BHE = bypass heat exchanger
CSP = concentrating solar power
HRU = heat rejection unit
HTF = heat transfer fluid
HTR = high temperature recuperator
LCOE = levelized cost of electricity
LTR = low temperature recuperator
MC = main compressor
PB = power block
PC = precompressor
PCC = partial cooling cycle
PHE = primary heat exchanger
P2P = POWDER2POWER
RCC = recompressed cycle
RCCB = recompressed cycle with HTR bypass
RCIC = recompressed cycle with intercooling
SAM = System Advisor Model
SC = secondary compressor
$sCO_2$ = supercritical carbon dioxide
SM = solar multiple
TES = thermal energy storage

## References

[1] IRENA, 2019, "Innovation Landscape Brief: Flexibility in Conventional Power Plants," International Renewable Energy Agency, Abu Dhabi, accessed May 1, 2024, https://www.irena.org/-/media/Files/IRENA/Agency/Publication/2019/Sep/IRENA_Flexibility_in_CPPs_2019.pdf?la=en&hash=AF60106EA083E492638D8FA9ADF7FD099259F5A1
[2] Binotti, M., Astolfi, M., Campanari, S., Manzolini, G., and Silva, P., 2017, "Preliminary Assessment of sCO$_2$ Cycles for Power Generation in CSP Solar Tower Plants," Appl. Energy, **204**, pp. 1007–1017.
[3] Bauer, T., Pfleger, N., Breidenbach, N., Eck, M., Laing, D., and Kaesche, S., 2013, "Material Aspects of Solar Salt for Sensible Heat Storage," Appl. Energy, **111**, pp. 1114–1119.
[4] IRENA, 2024, "Renewable Power Generation Costs in 2023," International Renewable Energy Agency, Abu Dhabi.
[5] Mehos, M., Turchi, C., Vidal, J., Wagner, M., Ma, Z., Ho, C., Kolb, W., Andraka, C., and Kruizenga, A., 2017, "Concentrating Solar Power Gen3 Demonstration Roadmap," National Renewable Energy Laboratory, Golden, CO, Report No. NREL/TP-5500-67464.
[6] Fernández, A. G., Ushak, S., Galleguillos, H., and Pérez, F. J., 2014, "Development of New Molten Salts With $LiNO_3$ and $Ca(NO_3)_2$ for Energy Storage in CSP Plants," Appl. Energy, **119**, pp. 131–140.
[7] Flamant, G., Grange, B., Wheeldon, J., Siros, F., Valentin, B., Bataille, F., Zhang, H., Deng, Y., and Baeyens, J., 2023, "Opportunities and Challenges in Using Particle Circulation Loops for Concentrated Solar Power Applications," Prog. Energy Combust. Sci., **94**, p. 101056.
[8] Siros, F., Valentin, B., Liu, B., Baeyens, J., and Flamant, G., 2022, "Next-CSP Concept With Particle Receiver Applied to a 150 MWe Solar Tower," Presented at the SOLARPACES 2020: 26th International Conference on Concentrating Solar Power and Chemical Energy Systems, Freiburg, Germany, Sept. 28–Oct. 2, p. 060006.
[9] Allison, T. C., Moore, J., Pelton, R., Wilkes, J., and Ertas, B., 2017, "7—Turbomachinery," *Fundamentals and Applications of Supercritical Carbon Dioxide (sCO2) Based Power Cycles*, K. Brun, P. Friedman, and R. Dennis, eds., Woodhead Publishing, Cambridge, MA, pp. 147–215.
[10] Musgrove, G., Sullivan, S., Shiferaw, D., Fourspring, P., and Chordia, L., 2017, "8—Heat Exchangers," *Fundamentals and Applications of Supercritical Carbon Dioxide (sCO2) Based Power Cycles*, K. Brun, P. Friedman, and R. Dennis, eds., Woodhead Publishing, Cambridge, MA, pp. 217–244.
[11] Alfani, D., Astolfi, M., Binotti, M., Campanari, S., Casella, F., and Silva, P., 2019, "Multi Objective Optimization of Flexible Supercritical $CO_2$ Coal-Fired Power Plants," ASME Paper No. GT2019-91789.
[12] Wagner, M. J., and Wendelin, T., 2018, "SolarPILOT: A Power Tower Solar Field Layout and Characterization Tool," Sol. Energy, **171**, pp. 185–196.
[13] Wendelin, T., 2009, "SolTRACE: A New Optical Modeling Tool for Concentrating Solar Optics," ASME Paper No. ISEC2003-44090.
[14] Gueguen, R., Grange, B., Bataille, F., Mer, S., and Flamant, G., 2020, "Shaping High Efficiency, High Temperature Cavity Tubular Solar Central Receivers," Energies, **13**(18), p. 4803.
[15] Behar, O., Grange, B., and Flamant, G., 2020, "Design and Performance of a Modular Combined Cycle Solar Power Plant Using the Fluidized Particle Solar Receiver Technology," Energy Convers. Manage., **220**, p. 113108.
[16] Morosini, E., Gentile, G., Binotti, M., and Manzolini, G., 2022, "Techno-Economic Assessment of Small-Scale Solar Tower Plants With Modular Billboard Receivers and Innovative Power Cycles," J. Phys.: Conf. Ser., **2385**(1), p. 012109.
[17] Picotti, G., Cholette, M. E., Casella, F., Binotti, M., Steinberg, T. A., and Manzolini, G., 2022, "Dynamic Thermal Analysis of an External Cylindrical Receiver in an Object-Oriented Modelling Paradigm," AIP Conf. Proc., **2445**(1), p. 080007.

[18] Gal, A. L., Grange, B., Gueguen, R., Donovan, M., Peroy, J.-Y., and Flamant, G., 2020, "Particle Flow and Heat Transfer in Fluidized Bed-in-Tube Solar Receivers," AIP Conf. Proc., **2303**(1), p. 070002.
[19] Crespi, F., Gavagnin, G., Sánchez, D., and Martínez, G. S., 2017, "Supercritical Carbon Dioxide Cycles for Power Generation: A Review," Appl. Energy, **195**, pp. 152–183.
[20] Alfani, D., Astolfi, M., Binotti, M., and Silva, P., 2021, "Part-Load Strategy Definition and Preliminary Annual Simulation for Small Size $sCO_2$-Based Pulverized Coal Power Plant," ASME J. Eng. Gas Turbines Power, **143**(9), p. 091026.
[21] Alfani, D., Binotti, M., Macchi, E., Silva, P., and Astolfi, M., 2021, "$sCO_2$ Power Plants for Waste Heat Recovery: Design Optimization and Part-Load Operation Strategies," Appl. Therm. Eng., **195**, p. 117013.
[22] Weiland, N., and Thimsen, D., 2016, "A Practical Look at Assumptions and Constraints for Steady State Modeling of $sCO_2$ Brayton Power Cycles," National Energy Technology Laboratory (NETL), Pittsburgh, PA/Morgantown, WV, Report No. NETL-PUB-20271, accessed Jan. 5, 2024, https://www.osti.gov/biblio/1491086
[23] Alfani, D., Neises, T., Astolfi, M., Binotti, M., and Silva, P., 2022, "Techno-Economic Analysis of CSP Incorporating $sCO_2$ Brayton Power Cycles: Trade-Off Between Cost and Performance," AIP Conf. Proc., **2445**(1), p. 090001.
[24] Audet, C., and Dennis, J. E., 2002, "Analysis of Generalized Pattern Searches," SIAM J. Optim., **13**(3), pp. 889–903.
[25] Weiland, N. T., Lance, B. W., and Pidaparti, S. R., 2019, "$sCO_2$ Power Cycle Component Cost Correlations From DOE Data Spanning Multiple Scales and Applications," ASME Paper No. GT2019-90493.
[26] Astolfi, M., 2014, "An Innovative Approach for the Techno-Economic Optimization of Organic Rankine Cycles," Ph.D. thesis, Politecnico di Milano, Milano, Italy, accessed Jan. 5, 2024, https://www.politesi.polimi.it/handle/10589/89363
[27] Peters, M., 2013, *Plant Design and Economics for Chemical Engineers*, 5th ed., McGraw-Hill, New York.
[28] Blair, N., DiOrio, N., Freeman, J., Gilman, P., Janzou, S., Neises, T., and Wagner, M., 2018, "System Advisor Model (SAM) General Description (Version 2017.9.5)," National Renewable Energy Laboratory, Golden, CO, Report No. NREL/TP-6A20-70414.
[29] Buck, R., and Giuliano, S., 2019, "Solar Tower System Temperature Range Optimization for Reduced LCOE," AIP Conf. Proc., **2126**(1), p. 030010.
[30] Gueguen, R., Sahuquet, G., Tessoneaud, M., Sans, J.-L., Guillot, E., Le Gal, A., Garcia, R., et al., 2023, "Heat Transfer in a Fluidized Bed Tubular Solar Receiver. On-Sun Experimental Investigation," Sol. Energy, **265**, p. 112118.
[31] Frantz, C., Buck, R., and Amsbeck, L., 2022, "Design and Cost Study of Improved Scaled-Up Centrifugal Particle Receiver Based on Simulation," ASME J. Energy Resour. Technol., **144**(9), p. 092107.
[32] Ho, C. K., 2016, "A Review of High-Temperature Particle Receivers for Concentrating Solar Power," Appl. Therm. Eng., **109**, pp. 958–969.
[33] Ho, C. K., Christian, J., Yellowhair, J., Jeter, S., Golob, M., Nguyen, C., and Repole, K., et al., 2017, "Highlights of the High-Temperature Falling Particle Receiver Project: 2012–2016," Presented at the SOLARPACES 2016: International Conference on Concentrating Solar Power and Chemical Energy Systems, Abu Dhabi, UAE, Oct. 11–14, p. 030027.
[34] Neises, T., and Turchi, C., 2019, "Supercritical Carbon Dioxide Power Cycle Design and Configuration Optimization to Minimize Levelized Cost of Energy of Molten Salt Power Towers Operating at 650 °C," Sol. Energy, **181**, pp. 27–36.